Synchronization of Legacy 802.11a/g Devices Operating in IEEE 802.11n Networks

Roger Pierre Fabris Hoefel and André Michielin Câmara

Department of Electrical Engineering,
Federal University of Rio Grande do Sul (UFRGS)
Porto Alegre - Brazil
roger.hoefel@ufrgs.br, andre.camara@ufrgs.br

Abstract—**It is investigated the performance of legacy IEEE 802.11a time synchronization algorithms when the synchronization preamble is transmitted by IEEE 802.11n devices with multiple transmitting antennas using cyclic shift diversity. It is concluded that the backward compatibility is achieved when the time synchronization is implemented using an auto-correlation maximum normalization metric.**

Keywords – 802.11n, 802.11a/g; synchronization.

I. INTRODUCTION

The IEEE 802.11n standard, which final version was ratified in September 2009, provides data rates up to 600 Mbps. The physical layer (PHY) is based on multiple-input multiple-output (MIMO) antennas in order to implement spatial division multiplexing (SDM), with the transmission of multiple spatial streams of information [1, p. 85]. The medium access control layer (MAC) uses advanced protocols (e.g., frame aggregation, block acknowledgment) that decrease substantially the overhead of the plain 802.11 MAC protocol [2]. The 802.11n networks operate with channel bandwidths of *20 MHz* and *40 MHz* at *2.4 GHz* and *5 GHz* Industrial, Scientific and Medical (ISM) bands. The fundamental backward compatibility with IEEE 802.11a/g amendments is implemented at PHY as follows: the high throughput (HT) 802.11n station (STA) transmits a mixed format (MF) preamble that can be decoded by 802.11a/g legacy devices. If the decoding is successful, then the legacy devices remain in the idle state during the time that the HT 802.11n device is loading the channel.

A challenging issue during the development of IEEE 802.11n standard was to define how to transmit the legacy preamble over multiple antennas since the HT device supports spatial multiplexing with up to four transmitting antennas and the preamble is a single stream signal. If the legacy preamble would transmit using just one antenna of HT device, then it would result in a drastic reduction of the transmitted power (e.g., one-fourth of the available power for HT devices with four transmitter antenna chains). On the other hand, transmitting the same signal on different antennas could result in undesirable beamforming effects due to the spatial combination of the transmitted signal at receiver input. The achieved solution is to transmit the legacy preamble using all available antennas (i.e., avoiding power lost), but using a cyclic shift diversity (CSD) scheme to decorrelate the signal transmitted at different antennas (i.e., avoiding beamforming effects).

In this paper, we use analytical and simulation tools to investigate the performance of 802.11a legacy devices operating in 802.11n networks over different channel models. Section II summarizes related works. Section III presents the 802.11n MF preamble. Section IV describes synchronization schemes for legacy 802.11a devices. Section V derives a first order analytical model used to validate the simulation results obtained with an IEEE 802.11n simulator that we have been developing. Section VI shows the performance of different synchronization schemes. The conclusions are drawn in Section VII.

II. RELATED WORKS

Perahia and *Stacey* [1, p. 72] described the schemes proposed during the 802.11n standard development in order to allow legacy compatibility without power lost and beamforming effects. One proposed approach was the tone-interleaving scheme, where the legacy preamble is transmitted in all antennas, but each antenna using only a subset of orthogonal frequency division multiplexing (OFDM) subcarriers. This scheme solves the problem of undesirable beamforming, but creates power fluctuation at receiver side. Notice that for an HT STA with four antennas just few subcarriers would be sent at each one and, therefore, there would be few tones in each stream to cover the entire signal bandwidth.

The adopted solution was the CSD technique, where the HT devices use the same subcarriers in each transmitting antenna, but with a phase shift to decorrelate the signal from different antennas, reducing the beamforming effects [3]. The main drawback of CSD scheme is the possible performance degradation of legacy 802.11a synchronization schemes, because the signal transmitted over multiple antennas generates multipath fading that the legacy 802.11a receiver must cope with. *Aoki*, *Egashira* and *Takeda* [3] show simulation results on performance of legacy 802.11a synchronization schemes assuming an HT transmitter with only two antennas and perfect channel estimation. Basically, this paper focused on automatic gain control (AGC) performance degradation due to power disparity between legacy and non-legacy part of HT preamble. *Selvam and Srikanth* [4] evaluated the performance of IEEE 802.11n networks operating in presence of 802.11a/g devices to assess the effects of the MF preamble overhead on the HT 802.11n network throughput.

III. MIXED FORMAT IEEE 802.11N PACKET STRUCTURE

Fig. 1 shows the HT 802.11n MF packet structure. The first three fields contain non-high throughput (non-HT) fields identical to 802.11a/g amendments: the Legacy Short Training field (L-STF); the Legacy Long Training field (L-LTF); and the Legacy Signal field (L-SIG) [5, pp. 275-278]. The L-STF has a length of *8 μs* (or *160* samples at a sample rate of *20 MHz* or sample period T_s equal to *50 ns*), comprising ten repetitions of a short symbol with period of *16* (*160/10*). The L-LTF also has a length of *8 μs (160 samples at T_s=50 ns)*, but with just two repetitions of a long symbol with *3.2 μs* each (or 64 samples at T_s=50 ns), and a cyclic prefix (CP) of *1.8 μs (32 samples at T_s=50 ns)* inserted to avoid inter-symbol interference (ISI) in multipath channels. The L-LTF has a period of *64 (160/2.5)*.
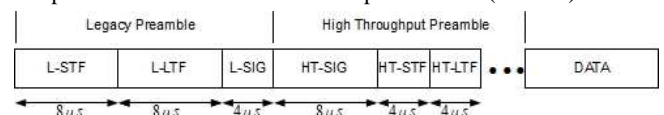

Fig. 1. Mixed format (MF) packet structure [5, p. 262].

The L-STF and L-LTF fields are used by 802.11a/g devices to time synchronization, AGC, frequency offset correction and channel estimation, as described in section IV. The L-SIG carries information about packet rate and length. The L-SIG consist of *24* information bits that are transmitted using binary phase-shift keying (BPSK) modulation and rate $r=½$ binary convolutional code (BCC), followed by interleaving [1, p. 64]. The legacy 802.11a/g devices must decode

the L-SIG to set its network allocation vector (NAV) in order to remain in the idle state during the atomic cycle time in which an HT device is loading the channel. The non-HT STA can only decode the frame until this point because the next fields are HT ones. A full description of HT fields is out of scope of this paper, and can be found in [1, p.70].

The CS applied on the transmitted OFDM symbol *s(t)* over a OFDM symbol length *T* is given by [5, p. 275]

$$s_{cs}(t, T_{CS})|_{T_{CS}<0} = \begin{cases} s(t - T_{CS}), & 0 \le t < T + T_{CS} \\ s(t - T_{CS} - T), & T + T_{CS} \le t < T \end{cases}. \quad (1)$$

Table I shows the values of the cyclic shifts T_{CS} defined in the IEEE 802.11n standard [5, p.276], where N_{TX} is the number of transmitting antennas.

TABLE I
CYCLIC SHIFTS FOR THE LEGACY PORTION OF THE MF PREAMBLE

N_{Tx}	T_{CS} (ns) Tx chain 1	T_{CS} (ns) Tx chain 2	T_{CS} (ns) Tx chain 3	T_{CS} (ns) Tx chain 4
1	0	----	----	----
2	0	-200	----	-----
3	0	-100	-200	----
4	0	-50	-100	-150

IV. SYMBOL SYNCHRONIZATION TECHNIQUES FOR OFDM

Time synchronization is the procedure of acquiring the time when each OFDM symbol start and end. We shall describe time synchronization algorithms based on the 802.11a standard since, as we have emphasized, the main objective of this paper is to assess the capability of legacy 802.11a devices to detect the L-SIG field (see Fig. 1) transmitted by HT 802.11n devices. Table I shows the major characteristics of IEEE 802.11a standard.

TABLE II
IEEE 802.11A SYSTEM PARAMETERS.

Parameter	Symbol	Value
Channel Bandwidth	W	20 MHz
Sampling Period	T_s	50 ns
Channel Subcarriers / FFT length	N_{FFT}	64
Data Subcarriers	N_{data}	48
Pilot Subcarriers	N_{pilot}	4
Subcarrier Spacing	$\Delta_F = W/N_{FFT}$	312.5 kHz
Symbol Period	$T = 1/\Delta_F + CP$	3.2 μs+800ns= 4 μs

Fig. 2 depicts the 802.11a preamble [6], where the STF and LTF fields have the same characteristics of the corresponding legacy fields shown in Fig. 1, except that now they are transmitted using just one antenna (i.e., the CSD scheme is not used). It is shown the ten short symbols, indicated by S1-S10 and the two long symbols, L1 and L2, with the cyclic prefix CP.
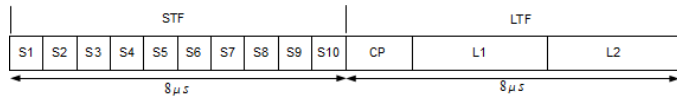

Fig. 2. The IEEE 802.11a preamble.

Considering that the packet has a random start time given by t_i, then the normalized time offset is [7, p.20]

$$\theta = \frac{t_i}{T_s}, \quad (2)$$

In this paper only integers values of θ are assumed, since fractional shifts would require an upsampled (i.e., more than *20 Msamples/s*) synchronization scheme, i.e., a highly demanding computational and power consumption load. The synchronization objective is to estimate θ. Fig. 3 shows a packet and three possible synchronization regions for the second received OFDM symbol, where $\Delta\theta$ is the difference between the estimated $\hat{\theta}$ and the correct θ.

For $\Delta\theta > 0$ and $\Delta\theta < -16$, it results in ISI and inter-carrier interference (ICI) since samples from the next or previous symbol, respectively, are used in the discrete Fourier transform (DFT) of the received symbol.
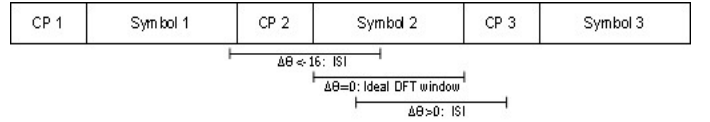

Fig. 3. DFT window position for three synchronization regions.

Assuming no ISI and ICI, the DFT of received signal is given by

$$R_k = DTF\{s[n - \Delta\theta]\} = S_k e^{-j2\pi k\Delta\theta/N_{FFT}}. \quad (3)$$

Eq. (3) shows that a lack of perfect time synchronization originates a linear phase offset that is not constant for all subcarriers. However, this phase offset can be compensated by the channel equalization using the channel estimation results from LTF, or through phase estimation using pilot subcarriers. The maximum tolerable time offset is given by [7]

$$|\Delta\theta| \le \frac{N_{FFT}}{2\,\Delta p}, \quad (4)$$

where Δp is the distance of the subcarriers used in the phase estimation. In the 802.11a, the distance among each one the four pilots is $\Delta p = 14$, therefore $|\Delta\theta| \le 2.28$.

A. Auto-Correlation Symbol Timing Synchronization

The synchronization time $\hat{\theta}$ can be estimated by searching the maximum argument of the maximum normalized correlation (MNC) metric m_n^{MNC} [8]:

$$\hat{\theta} = \max_n(m_n^{MNC}) = \max_n\left(\frac{|c_n|^2}{(p_{n-N})^2}\right). \quad (5)$$

The auto-correlation of received signal r_n at *nth* sample is defined as

$$c_n = \sum_{i=0}^{L-1} r_{n+i}^* \, r_{n-N+i}, \quad (6)$$

where the parameter *N* is equal to or multiple of signal period, and *L* is equal to or multiple of *N*. The L-STF has a period of *16*, while the L-LTF has a period of *64*.

Eq. (5) shows that the MNC criteria use the received power in the correlation window (see Eq. 7) to normalize the correlation result in order to diminish its dependence with the received power.

$$p_{n-N} = \sum_{i=0}^{L-1} |r_{n-N+i}|^2. \quad (7)$$

Fig. 4 shows a simplified block diagram of the auto-correlation synchronization scheme, given by (5).
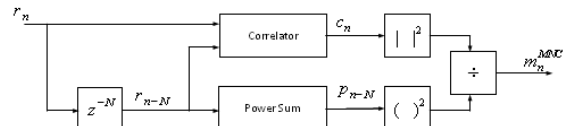

Fig. 4. Block diagram of the auto-correlation synchronization scheme.

Assuming no noise, the maximum value at the correlator output is given by

$$c_n^{max} = L\sigma_r^2, \quad (8)$$

where σ_r^2 is the received signal power. The average power of the received waveform at receiver input is given by

$$\sigma_r^2 = \frac{p_n}{L}. \quad (9)$$

Therefore, the maximum value of m_n^{MNC} is equal to 1 when there is no noise.

Figures 5a and 5b shows the MNC metric for AWGN channel with signal-to-noise ratio of 10 dB and 0 dB, respectively. Fig. 5c shows the MNC metric for a Rayleigh selective Rayleigh fading channel with a root mean square (RMS) delay spread of 200 ns and SNR of *10 dB*. The period of L-STF is *N=16*. Hence, using L=*144* allow obtaining a single peak that indicates the start of LTF since it is accumulated *9 (L/N)* L-STF. Notice that the frame has an initial delay of *500 samples* and, therefore the peak occurs at sample *660 (500+ number of STF samples)*.
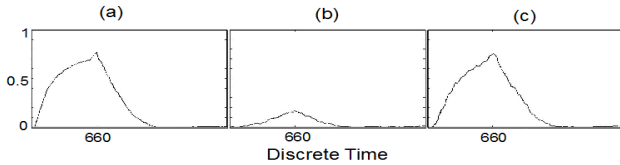
Fig. 5. MNC metric signal with $N=16$ and $L=144$: (a) AWGN channel with $SNR=10$ dB; (b) AWGN with $SNR=0$ dB and (c) selective Rayleigh fading with RMS delay spread of 200 ns and $SNR=10$ dB.

B. Cross-Correlation Symbol Timing Synchronization

The synchronization time $\hat{\theta}$ can be estimated by searching the maximum argument of metric m_n^{CC} [9, p. 61]:

$$\hat{\theta} = \max_n(m_n^{CC}) = \max_n\left(\frac{|d_n|^2}{p_n+p_s}\right). \tag{10}$$

The cross-correlation of received signal r_n and the pre-defined preamble s is defined as

$$d_n = \sum_{i=0}^{L-1} r_{n+i}^* s_i, \tag{11}$$

where the parameter L is the length of signal s.

Eq. (10) shows that the cross-correlation d_n is normalized by sum of the received waveform power p_n (see Eq. 7 with $N=0$) with the power of the reference stored signal p_s in order to avoid dependence with the received power.

Fig. 6 depicts a block diagram of cross-correlation synchronization scheme.
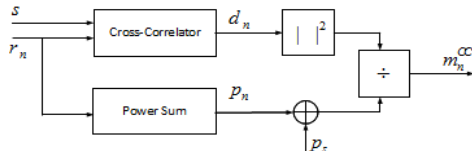

Fig. 6. Block diagram of the cross-correlation synchronization scheme.

A synchronization scheme based on cross-correlation requires three steps to acquire symbol synchronization. First, it is necessary to implement a packet detector, since the cross-correlation is a demanding numerical operation that must not be active all the time to save power. The detector is a simple auto-correlation given Eq. (5) with $N = 16$ and $L = 16$, resulting in a plateau during the reception of STF (see Fig. 7a). Once the correlator signalizes the arriving of a new packet, then a cross-correlation between the signal and a stored short symbol is performed. The result of cross-correlation is *10* *(160/16)* peaks indicating the position of each short symbol. As the stored signal has only $L=16$ samples, then cross-correlation metric is very susceptible to noise and fading. Therefore, a third step uses the LTF preamble to get the fine symbol synchronization. The cross-correlation metric uses one long symbol as stored signal, resulting in two peaks that estimate the position of each long symbol.

Fig. 7 shows the three steps of cross-correlation over AWGN channel and selective Rayleigh fading channels. The first column is the detector signal, indicating a presence of a packet. The second column is the cross-correlation of the signal with the L-STF (notice the 10 peaks) and the last one is the correlation with the stored L-LTF (notice the 2 peaks).

C. Auto-Correlation Versus Cross-Correlation Schemes

The auto-correlation scheme presents a lesser computation load since it can be computed recursively (see Equations 5-7). On the other hand, it uses a delay line of $L=144$ samples instead of a delay line of *L=16 samples* used by the cross-correlation scheme. Fig. 7c shows that the cross-correlation scheme presents a severe performance degradation in multipath fading channels since the received waveform is correlated with a "clear" stored preamble, resulting in loss of information. Notice that in this case there is a loss
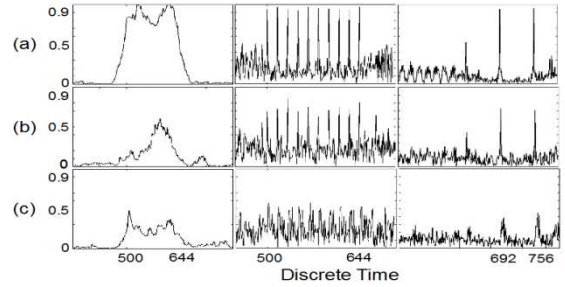

Fig. 7. The three steps of cross-correlation scheme for (a) AWGN channel with $SNR=10$ dB; (b) AWGN with $SNR=0$ dB and (c) selective Rayleigh fading with RMS delay spread of *200 ns* and $SNR=10$ dB.

of information since the received signal should be correlated with the convolution of the reference signal and channel impulsive response. Comparing Figures 5c with 7c, we can see that auto-correlation suffers just a small degradation with fading.

For AWGN channels, the correlation with a clear stored preamble makes the cross-correlation scheme more immune to additive noise in relation to the auto-correlation scheme, as we can see when comparing Fig. 5b and Fig. 7b for a $SNR=0$ dB.

V. FIRST ORDER ANALYTICAL RESULTS

A. Simulation Model

We have been developing a PHY and MAC cross-layer IEEE 802.11n [5] simulator using C++ and MatLab. The simulator also implements the IEEE 802.11a amendment [6].

The transmitter module follows the 802.11n standard, creating a baseband signal sent in each antenna. This contribution has focused on IEEE 802.11n and 802.11a compatibility issues. Therefore, the transmitted packet is generated until the L-SIG field, as described in Section III.

The simulations are performed over AWGN, flat fading Rayleigh and frequency selective Task Group n (TGn) MIMO channels [10]. The TGn models are a set of statistical based indoor MIMO models, where each model refers to a given environment class. It is assumed an underspread fading channel, i.e., the fading is constant during the transmission of whole packet. The simulator can also add the following impairments to the received signal: sampling offset, frequency offset, and phase noise. However, in this paper we focus only on time synchronization due to space constraints.

The legacy 802.11a receiver implements the channel estimation in the frequency domain using the L-LTF as follows. The kth subcarrier of lth received L-LTF symbol in frequency domain is given by

$$R_{l,k} = H_k L_{l,k} + W_{l,k}, \tag{12}$$

where H_k denotes the channel response for kth OFDM subcarrier, $L_{l,k}$ is the lth L-LTF symbol. The AWGN for kth subcarrier at lth symbol is denoted by $W_{l,k}$.

The L-LTF (see Fig. 2) has two symbols. Therefore, the first step to estimate the channel is to perform an average of both symbols to reduce the deleterious noise effect. Finally, the channel can be estimated by

$$\hat{H}_k = \frac{1}{2}\left(\frac{R_{1,k}+R_{2,k}}{L_k}\right). \tag{13}$$

The correlation among adjacent carriers is utilized to improve the channel estimation in low delay spread channels:

$$\tilde{H}_k = \frac{a\hat{H}_{k-1}+b\hat{H}_k+a\hat{H}_{k+1}}{2a+b}, \tag{14}$$

where the weights values are found heuristically through simulation, resulting in $a = 1$ and $b = 2$.

It is used a zero forcing (ZF) equalization at each subcarrier of the L-SIG field. Finally, a hard decision Viterbi decoder is used to detect the information carried on the L-SIG field.

B. Analytical Model for L-SIG Error Rate

Assuming that the convolutional code is decoded using hard-decision Viterbi decoder, then (15) models the probability of incorrectly selecting a path when the Hamming distance d is even [11]. The used notation emphasizes the dependence of P_d with the effective received SNR per coded symbol γ_c and the *PHY mode m* [1, p.64]. The average raw bit error rate (BER) at the Viterbi decoder input for the *PHY mode m* modulation scheme is denoted by ρ_m.

$$P_d(\gamma_c, m) = \frac{1}{2}\binom{d}{d/2}\rho_m^{d/2}(1-\rho_m)^{d/2} + \sum_{k=\frac{d}{2}+1}^{d}\rho_m^k(1-\rho_m)^{d-k}. \quad (15)$$

Considering the BCC 802.11a generator polynomials, $g_0=(133)_8$ and $g_1=(171)_8$, with code rate $r=1/2$ and constraint length $K=7$ [6, p.16], then the union bound on the probability of decoding error is given by

$$P_e(\gamma_c, m) = 11P_{10}(\gamma_c, m) + 38P_{12}(\gamma_c, m) + 193P_{14}(\gamma_c, m). \quad (16)$$

When the errors inside of the decoder are dependent, then *Pursley* and *Taipale* have shown that the upper bound for a successful transmission of a frame with l bits is given by [12]

$$S(l, \gamma_c, m) < [1 - P_e(\gamma_c, m)]^l. \quad (17)$$

For a block-fading channel (or underspread channel), this upper bound can be modified to [11]

$$S(l, \gamma_c, m) < \int_{\gamma_{inf}}^{\infty}[1 - P_e(\gamma_c, m)]^l p(\gamma_c)d\gamma_c \quad (18)$$

where the lower limit of the definite integral is chosen so that

$$[1 - P_e(\gamma_c, m)]^l \leq 1 \; for \; \gamma_c \geq \gamma_{inf}. \quad (19)$$

Considering Nakagami-m fading, **c**hannel diversity with L independent branches with the same average received power, then the probability distribution function (pdf) of the SNR per bit at the detector input is Gamma kind [11]

$$p(\gamma_c) = \frac{1}{\Gamma(L\,m_n)}\left(\frac{m_n}{\overline{\gamma_c}}\right)^{L\,m_n}(\gamma_b)^{L\,m_n-1}\,exp\left(-\frac{m_n\gamma}{\overline{\gamma_c}}\right) \; if \; \gamma > 0, \, mn \geq 0.5, \quad (20)$$

where m_n is the Nakagami-m fading figure ($m_n=1$ for Rayleigh), $\overline{\gamma_c}$ denotes the average SNR per coded symbol at the Viterbi decoder input.

It has been assumed hard decision of BPSK symbols, then the raw BER for the *k-th* OFDM subcarrier at decoder input is given by

$$\rho_k = Q(\sqrt{2\gamma_c}), \quad (21)$$

where the effective SNR per symbol is given by

$$\gamma_c = \frac{E_b}{N_0} \cdot r \cdot \left(\frac{T}{T+T_{prefix}}\right) \cdot \frac{N_{FFT}}{N_{data}+N_{pilot}} \cdot \frac{1}{N_{TX}}. \quad (22)$$

It is used the following notation in (21): E_b is the energy per bit; N_0 is one-side noise spectral density; $T_{prefix}=800 \, ns$ is the cyclic prefix length; T, N_{FFT}, N_{data} and N_{pilot} are given in Table II.

VI. NUMERICAL RESULTS

In this section we shall show analytical and simulation results for the L-SIG decoding error assuming no frequency offset. However, it is analyzed the effects of non-ideal symbol synchronization scheme over AWGN, flat and frequency selective Rayleigh fading channels. In all simulations, it is used a legacy 802.11a receiver with just one antenna, and an HT 802.11n transmitter with the number of antennas varying from *1* to *4*.

Fig. 8 shows the L-SIG error rate as function of SNR per bit. It is assumed a legacy 802.11a receiver with *perfect synchronization* over an AWGN channel. It is shown results with and without ZF equalization, parameterized by the number of transmitting antennas. For $N_{TX}=1$ the channel equalization inserts a small degradation on the performance since the channel is AWGN. However, we can see that if the ZF equalization is not implemented, then there is a strong degradation (proportional to the number of transmitting antennas) on the L-SIG decoding error when it is used more than one transmitting

antenna. Notice that for the ZF receiver the L-SIG error rate presents similar results for $N_{TX}=3$ and $N_{TX}=4$ antennas, with the last one being a slight better. Notice that for *4* antennas the maximum CS applied is lower than for *3* antennas (see Table I). Therefore, as CSD is observed at the receiver input as a multipath, then there is a worst performance for larger cyclic shifts. Hereafter, we shall only present results with ZF receiver since we have concluded the system does not work properly without channel correction even in AWGN channels when it is implemented the CSD transmitting scheme.
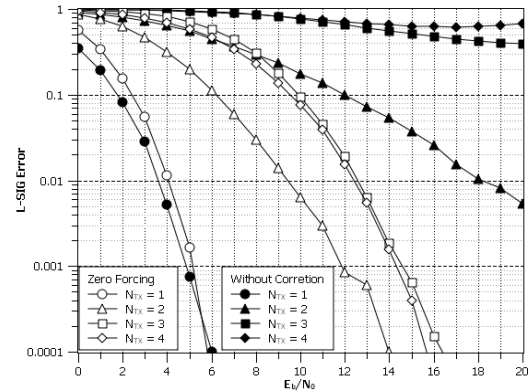

Fig. 8. L-SIG error rate versus SNR per bit over AWGN channel using a receiver with *perfect synchronization*.

Fig. 9 shows the L-SIG error rate as a function of SNR per bit over an AWGN channel. There is an excellent agreement between analytical and simulation results for perfect synchronization with just one transmitting antenna. Assuming $N_{tx}=1$ and a packet loss rate of *1%*, we have verified a degradation of approximately *1 dB* (*2 dB*) for auto-correlation (cross-correlation) synchronization scheme. We can see that the error rate increases as the antennas number increase. For both synchronization schemes, the L-SIG decoding error rate is worse with $N_{TX}=3$ than with $N_{TX}=4$ since as a greater delay is applied for $N_{tx}=3$, as explained earlier.

Fig. 9 also shows that there is a catastrophic degradation on the system performance when it is used a cross-correlation synchronization scheme with $N_{tx}=3$. As mentioned in Section IV, the cross-correlation is very sensible to multipath. Hence, for $N_{tx}=3$ the channel is observed at receiver as multipath channel with resolution of three paths. This divides the power of the correlation in three peaks, with lower amplitudes that make difficult to the detector to identify the peaks with confidence. For $N_{TX}=4$ this phenomenon does not occur due to the smaller CS, which is not sufficient to spread significantly the power of correlation peaks.
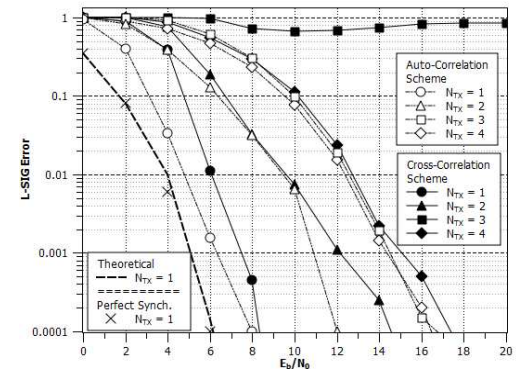

Fig. 9. L-SIG error rate versus SNR per bit over AWGN channel.

Fig. 10 shows the L-SIG error rate as a function of SNR per bit over a flat fading Rayleigh channel. We can see that for $N_{Tx}=1$ the simulation results are in agreement with the analytical upper bound, which was derived assuming perfect synchronization. In this case, we

can also notice a similar performance for auto and cross-correlation synchronization schemes. The L-SIG error rate _decreases substantially_ when the number of transmitter antennas increases. This occurs because the CSD scheme jointly with interleaving transforms a flat fading channel into an observable frequency selective channel at detector input. For the auto-correlation scheme the best result is achieved with $N_{TX}=4$. With the cross-correlation scheme the performance for $N_{TX}=3$ and $N_{TX}=4$ are almost identical until a SNR of _14 dB_, where the performance with four antennas degrades due to the self-interference. Finally, notice that the auto-correlation scheme allows a better performance than the cross-correlation scheme, independent of the number of transmitting antennas and SNR per bit.
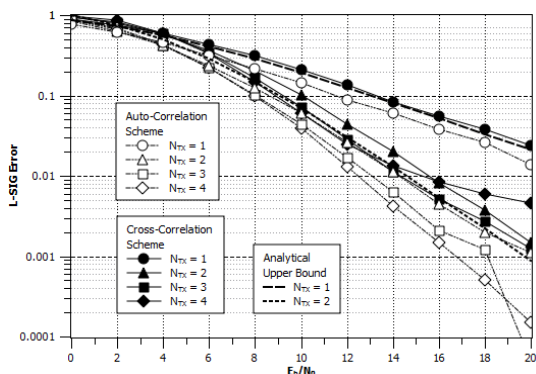

Fig. 10. L-SIG error rate vs SNR per bit over a flat fading Rayleigh channel.

Fig. 11 shows the L-SIG error rate as a function of SNR per bit over a Rayleigh frequency selective channel with an exponential power delay profile and a RMS delay spread of _100 ns_ (i.e., it models large office environments) and channel resolution of _50 ns_. It is noticed again that the use a HT transmitter with CSD allows an improvement on performance of the legacy 802.11a receiver when it is used an auto-correlation synchronization scheme. Again, the performance is degraded when it is used a cross-correlation synchronization scheme due to the cross-correlation of the received signal with a reference signal without channel information.
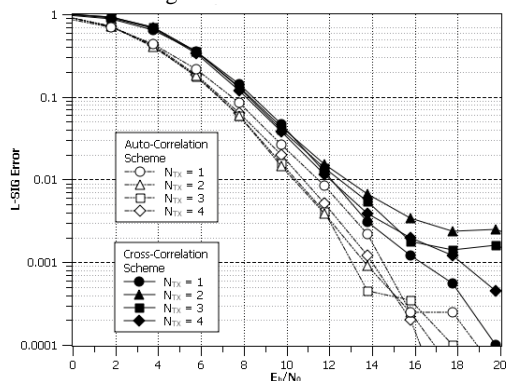

Fig. 11. L-SIG error rate versus SINR over a frequency selective Rayleigh channel with an exponential power delay profile and delay spread of 100 ns.

Finally, we present results for the TGn channel model 'E', which have a minimum tap separation of _10 ns_, while the transmitted signal has a sampling period of _50 ns_. Thus, the signal is upsampled by a factor of _5_ at channel input to perform the convolution with the channel response. The result is downsampled with same rate at channel output, so the receptor uses the original system sampling frequency of _20 MHz_.

Fig. 12 shows the L-SIG error rate for the frequency selective _TGn channel model 'E'_, which has a RMS delay spread of 1_50 ns_. Notice that the now CSD technique degrades the performance for both the cross-correlation and auto-correlation synchronization schemes.

Notice that differently from the channel simulated at Fig. 11, the TGn channel model presents spatial correlation among the transmitted antennas. Finally, it is noticed for the L-SIG decoding error of _1%_ practically the same performance is obtained when it is used the auto-correlation synchronization scheme with one, two or three antennas.
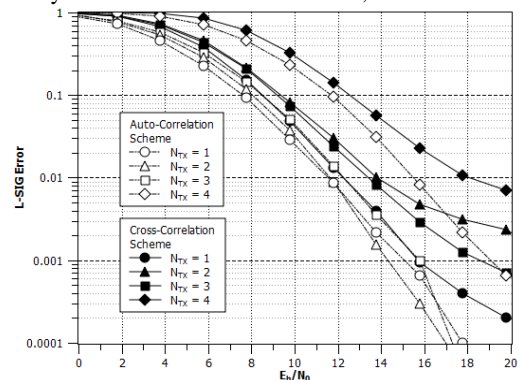

Fig. 12. L-SIG error rate versus SINR over a TGn channel model 'E'.

VI - CONCLUSIONS

We analyzed the performance using analytical and simualtion tools of two major synchronization schemes (i.e., auto-correlation and cross-correlation) in order to investigate the backward compatibility of legacy 802.11a devices operating in 802.11n networks. It was shown results for AWGN, flat fading Rayleig, Rayleigh frequency selective with exponential power delay profile and TGn 'E' channel models. We concluded that the auto-correlation synchronization scheme presents a superior performance in relation to the cross-correlation scheme and it allows the backward compatibility between IEEE 802.11n HT transmitter with CSD technique and legacy 802.11a/g receivers.

REFERENCES

[1] E. Perahia and R. Stacey, _Next Generation Wireless LANS_. New York, USA: Cambridge University Press, 2008.

[2] R. P. F. Hoefel. _"On IEEE EDCA 802.11n,"_ in The 6th International Symposium on Wireless Communication (ISWCS 2009), p. 478-482 Tuscany, Italy, 2009.

[3] T. Aoki, Y. Egashira and D. Takeda. _"Preamble structure for MIMO-OFDM WLAN systems based on IEEE 802.11a,"_ in IEEE 17th International Symposium on Personal, Indoor and Mobile Radio Communications, 2006, pp. 1-6, Sept. 2006.

[4] T. Selvam and S. Srikanth. _"Performance study of IEEE 802.11n WLANs,"_ in Communication Systems and Networks and Workshops, 2009. COMSNETS 2009, pp.1-6, Jan. 2009.

[5] IEEE 802.11n, _Part 11: Wireless LAN Medium Access Control (MAC) and Physical Layer (PHY) Specification – Amendment 5: Enhancements for Higher Throughput"_. Supplemented to IEEE 802.11 Standard, June, 2009.

[6] IEEE 802.11a, _Part 11: Wireless LAN Medium MAC and Phy Layer (PHY) Specification – Amendment 1: High-speed Physical Layer in the 5 GHz band"_. Supplemented to IEEE 802.11 Standard, Sept. 1999.

[7] R. Spitschka. _Synchronization Algorithms for OFDM Systems Using the Example of WLAN_. Saarbrucken, Germany VDM Verlag, 2008.

[8] T. M. Schimidl and D. C. Coax. _"Low overhead, low complexity [Burst] synchronization for OFDM,"_ in IEEE International Conference on Communication, vol. 5, p. 2777-2782, 1998.

[9] J. Heiskala and J. Terry, _OFDM Wireless LANs: A Theoretical and Practical Guide_. Indianapolis, USA: Sams Publishing, 2002.

[10] IEEE 802 11-03/161r2, TGn Indoor MIMO WLAN Channel Models.

[11] R. P. F. Hoefel. _"Goodput and delay cross-layer analysis of IEEE 802.11a networks over block fading channels,"_ in Proc. of IEEE Consumer Comm. Networking Conf. 2006, Las Vegas, USA. 2006.

[12] M. B. Pursle and D. J. Taipale. _"Error probabilities for spread-spectrum packet radio with convolutional codes and Viterbi decoding,"_ IEEE _Trans. Commun,_ vol. 35, n. 1, p. 1-12, Jan. 1987.